Journal of Imaging Science and Technology® 69(3): 1–8, 2025.

Carbon Black/Graphene Paper-based Flexible Sensors: Finite Element Simulation and Properties

Zhicong Tian, Ruien Yu, and Yanan Zeng
Shanxi Key Laboratory of Advanced Manufacturing Technology, North University of China, Taiyuan 030051, China
E-mail: yuruien@nuc.edu.cn

Jingbo Hu
Faculty of Printing, Packaging Engineering and Digital Media Technology, Xi'an University of Technology, Xi'an 710054, China

Haijun Gong
Shanxi Shouyang Duanwang Coal Industry Group Co., Ltd, Jinzhong 045400, China

Xijing Zhu
Shanxi Key Laboratory of Advanced Manufacturing Technology, North University of China, Taiyuan 030051, China

Abstract. *In recent years, with the rise of printed electronics technology, printed flexible sensors have garnered widespread attention. To predict the performance of sensors before actual fabrication, in this paper, the bending strain and resistance response of the sensor's functional layer were simulated using COMSOL Multiphysics 6.0 software, and the effects of different carbon black/graphene fill ratios on the sensor's bending performance were explored. The simulation results indicated that resistance increases with the bending angle during the bending process, and the bending-resistance characteristics are better when the carbon black to graphene mass ratio is 2:1. Subsequently, flexible strain sensors were fabricated using screen-printing technology and their bending performance was tested. The experimental results demonstrated that the sensors have good linearity ($R^2 = 0.9851$), favorable response and recovery times (approximately 1 and 2 s, respectively), low hysteresis (4.88%), and better cyclic stability when repeatedly bent at $0^\circ - 20^\circ$ compared to $0^\circ - 90^\circ$. The experimental results were consistent with the simulation results. This study provides a new perspective on the design of flexible strain sensors through synchronized experiments and simulations, which is expected to significantly reduce the cost of prototype development.*

Keywords: *printed electronics, strain sensors, finite element simulation, strain-resistive effect*

[DOI: 10.2352/J.ImagingSci.Technol.2025.69.3.030401]

1. INTRODUCTION

With the advancement of technology, traditional sensors are limited by the characteristics of their materials and cannot withstand large deformations, which restricts their application in the field of curved and irregular surfaces. Therefore, the research on flexible sensors made from materials that are soft, bendable, and stretchable, capable of bending and adapting to surface shapes, has a promising future [1]. Many researchers have already started exploring this field, which includes wearable devices [2–5], motion detection [6], medical health monitoring [7], and so on. The development of flexible strain sensors is continuously expanding the boundaries of sensor technology applications, promoting innovation and progress in many industries.

Selecting the right conductive functional materials is the foundation for achieving high-performance flexible sensors. Conductive composite materials, which are made by adding conductive fillers to a flexible polymer matrix, are commonly used to prepare functional layer materials for flexible sensors due to their good flexibility, and mechanical and electrical properties [8]. Metal nanomaterials and carbon materials are often used as conductive materials [9]. Among them, carbon materials such as carbon black, graphene, and carbon nanotubes are often used as conductive fillers due to their advantages of low cost, good conductivity, and high chemical stability [10]. The properties of the flexible polymer matrix can regulate the mechanical properties of the conductive composite material, such as strength and toughness [11], which is crucial for meeting the needs of different applications. Polymer matrices, such as polydimethylsiloxane (PDMS) [12], polyvinylidene fluoride [13], and thermoplastic polyurethane [14], serve as solid support bodies in conductive composite materials, providing structural support for conductive fillers and helping to maintain their dispersion, thereby forming a stable composite material structure.

Currently, flexible strain sensors that are commonly constructed typically include resistive and capacitive types, among which resistive sensors are widely studied due to their simple device structure, high sensitivity, simple reading mechanism, and low energy consumption [15]. Yi et al. [16] designed and manufactured a low-cost piezoresistive sensor by directly placing a solidified carbon ink film on liquid PDMS followed by a drying process for adhesion to prepare an ultra-thin film strain sensor. In tensile tests, when the

---

Received June 19, 2024; accepted for publication Sept. 2, 2024; published online Oct. 8, 2024. Associate Editor: Li Yang.

1062-3701/2025/69(3)/030401/8/$25.00

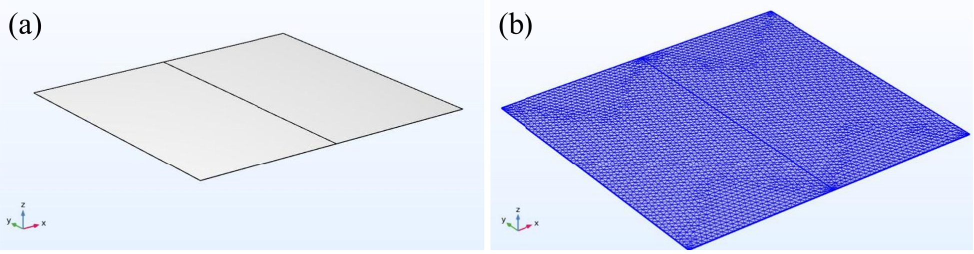

Figure 1. The (a) sensor model and (b) model mesh division diagram.

strain reaches 5%, the sensor's resistance change rate can be as high as about 122%, and the experimental results also prove the stability, repeatability, and consistency of the resistance change rate response to strain changes. Zhang et al. [17] proposed mixing carbon nanofibers and graphene nanoplatelet conductive fillers in a PDMS matrix, and prepared a highly flexible sandwich strain sensor with higher sensitivity and stability using spin coating. Xiao et al. [18] used a simple and low-cost screen-printing technique to print a polyvinyl chloride/carbon black composite on a polyimide substrate, preparing a high-performance crack-based flexible strain sensor. Long et al. [19] used molybdenum carbide–graphene composites as sensing materials and manufactured a paper-based strain sensor using a laser direct writing method on a paper substrate. This sensor has the characteristics of high sensitivity, fast response/recovery time, and good stability, and can be used to detect and recognize various types of human motion.

Although many flexible sensors have excellent performance, they have undergone numerous experimental parameter optimizations and have a long preparation cycle. The performance of printed flexible sensors is influenced by various factors, such as the filling ratio of conductive materials, the choice of substrate materials, and printing processes. To optimize the performance of the sensors, it is necessary to conduct in-depth research on these factors. Traditional experimental methods are time-consuming and labor-intensive, and the cost is relatively high. Therefore, using simulation technology to predict and optimize the performance of sensors has become an effective research method [20–22].

To minimize design and testing costs while comprehensively and accurately assessing the bending-resistance characteristics of flexible sensors, this study employs a combined approach of simulation and experimentation to investigate these properties. Initially, different carbon black/graphene mass ratios in the functional layer are virtually tested under various angle stresses and resistance changes using COMSOL Multiphysics 6.0 software, pinpointing the optimum carbon black/graphene mass ratio. Subsequently, functional ink is prepared according to the optimal mass ratio determined by simulations. Lastly, flexible sensors are fabricated using screen-printing techniques, with their bending performance studied, yielding paper-based sensors characterized by high sensitivity and rapid response. This research endeavors to provide theoretical foundations and experimental data support for the design and optimization of printed flexible sensors, thereby facilitating further advancements in printed electronics technology within the sensor domain.

2. SIMULATION AND SENSOR FABRICATION

2.1 *Modeling and Preprocessing*

The simulation process involved establishing a geometric model, constructing physical fields, selecting materials and defining material properties, setting boundary conditions, meshing, and analyzing results. First, a three-dimensional structure was selected in the Model Wizard. The device model was constructed within the Geometry Plane function in COMSOL Multiphysics 6.0, creating a model with dimensions of 16000 × 15000 × 20 μm. Then, a working plane was created to divide the rectangle into two halves, thus completing the construction of the three-dimensional model as shown in Figure 1(a). Subsequently, the geometric model was used to construct physical fields. The physical fields were set to the Solid Mechanics module and the Electric Currents module. The Solid Mechanics module was used for changing the angle of bending strain to study the effect of bending strain on the sensor's resistance. During the simulation, one side of the model was fixed, and the other side was bent to 30°, 60°, and 90°. Then, material properties were set. An empty material was selected, and the parameters for the required carbon black/graphene/PDMS composite material were filled in the corresponding positions. The material was chosen for all domains so that the rectangle was endowed with this composite material. Next, boundary conditions and constraints were set according to the actual bending conditions.

In COMSOL Multiphysics 6.0, meshing is very important as it directly affects the accuracy, stability, and computational efficiency of simulations. A more uniform and appropriate mesh can more accurately describe the geometric shape and boundary conditions of the simulated object, thereby producing more reliable simulation results; it can reduce computational costs while maintaining accuracy, thus speeding up the simulation run; it can also ensure the numerical stability of the simulation, as inappropriate or insufficient mesh may lead to issues such as numerical instability, simulation crashes, or slow convergence. This model is quite regular, and a conventional triangular mesh was selected to divide the model as shown in Fig. 1(b).

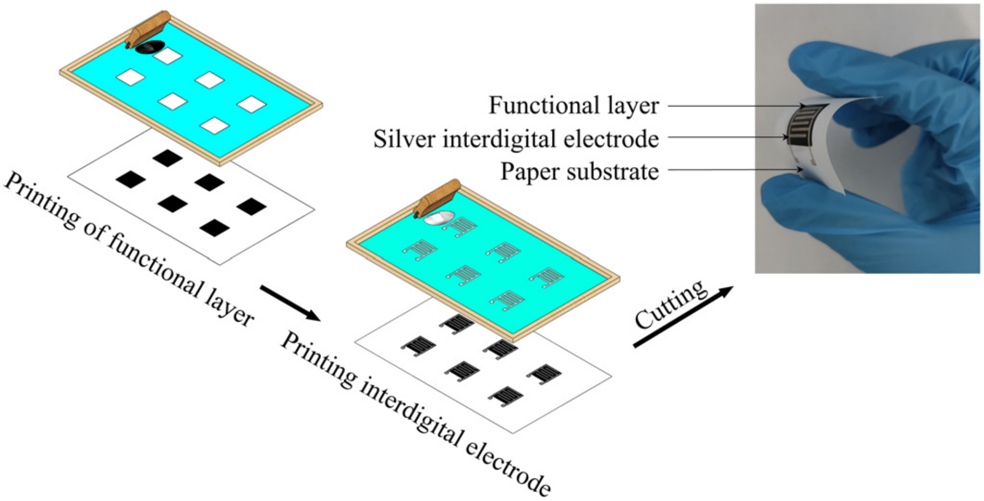

Figure 2. Preparation process of flexible sensors.

Table I. Reagents and chemicals used in the experiment.

Name	Specification	Supplier
Carbon black	BP2000	Cabot Corporation, USA
Graphene	Single layer, carbon content 98%	Shenzhen Suiheng Technology Co., Ltd.
Anhydrous ethanol	Analytically pure	Shanghai Ke Lin Biochemical Technology Co., Ltd.
PDMS	Sylgard 184	Dow Corning Corporation, USA
Conductive silver paste	Resistivity: 25 mΩ; Viscosity: 200∼300 Pa·s	Xinda Advanced Materials Co., Ltd.

After completing the aforementioned steps, the simulation is finally run to obtain the results.

2.2 *Preparation of Functional Inks*

The reagents and chemicals used in the experiment are shown in Table I. First, a certain mass of carbon black (Cabot Corporation, USA) and graphene (Shenzhen Suiheng Technology Co., Ltd.) was weighed to ensure that their total mass accounted for 4.0 wt% of all the ingredients, and then mixed with 10 g of anhydrous ethanol (analytically pure) and dispersed ultrasonically in an ultrasonic cleaner (Kunshan City Ultrasonic Instrumentation Co., Ltd.) for 20 min; second, a certain mass of PDMS (Dow Corning, Sylgard 184) was weighed and added to the above mixture for ultrasonic stirring for 30 min; subsequently, the curing agent was added to the mixture in accordance with m(PDMS)/m(curing agent) = 10:1 and ultrasonic stirring continued for 30 min, and the functional ink was prepared. Repeating the above steps and changing the filling mass ratio of carbon black and graphene to 1:0, 2:1, 1:1, 1:2, and 0:1, five groups of functional inks with different ratios were prepared.

2.3 *Preparation of Flexible Sensors*

The preparation of flexible sensors is based on manual screen-printing technology, and the preparation process is shown in Figure 2. The printing parameter for both the functional layer and the interdigital electrodes is a mesh count of 150 for the screen printing, with the printing done twice. Firstly, functional ink was used to form the functional layer of a flexible sensor on a paper substrate through screen printing technology. Subsequently, the printed sample was placed into an electrically heated air-circulating drying oven (Foshan Jinshen Electromechanical Equipment Co., Ltd.), where it was cured for 40 min. After the curing process was completed, the sample was allowed to cool to room temperature under natural conditions. Next, conductive silver paste was applied onto the already cured functional layer using screen printing technology to form interdigital electrodes. Finally, the sample with the interdigital electrodes was placed back into the electrically heated air-circulating drying oven and dried for 50 min, thereby completing the preparation of the flexible sensor. According to different filling mass ratios of carbon black and graphene, the prepared sensor samples were numbered 1#, 2#, 3#, 4#, and 5# as shown in Table II.

Table II. Sensor sample number information.

CB:graphene (mass ratio)	1:0	2:1	1:1	1:2	0:1
Sample number	1#	2#	3#	4#	5#

'CB stands for carbon black'

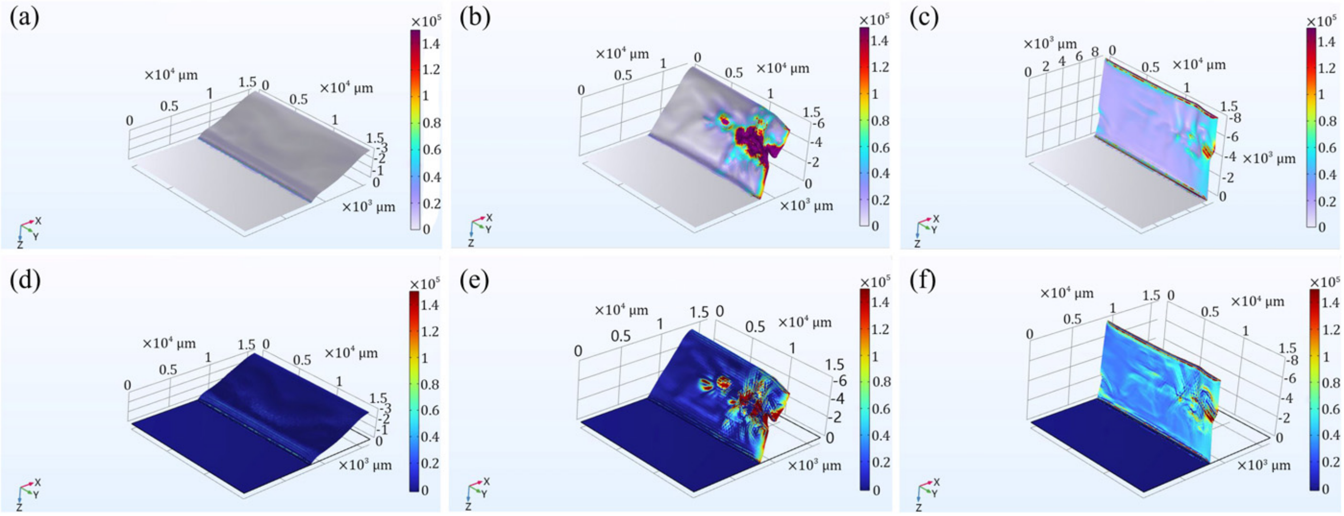

Figure 3. Simulation results of the bending-resistance characteristics of 1# sensor sample: (a) 30° bending stress diagram, (b) 60° bending stress diagram, (c) 90° bending stress diagram, (d) 30° bending-resistance change diagram, (e) 60° bending-resistance change diagram, and (f) 90° bending-resistance change diagram.

2.4 *Characterization and Testing*

The COMSOL Multiphysics 6.0 software was used to simulate the stress and resistance changes in the functional layer of the flexible sensors at 30°, 60°, and 90° of bending. The linearity of the flexible sensors at different bending angles from 10° to 90° was tested in steps of 10°. The resistance data were collected using a digital source meter (Keithley 2450, USA) as a way to record the resistance changes in the flexible sensors at different bending angles so as to obtain their bending-resistance characteristics. The sensors were also selected for cyclic bending tests at small angles of $0° - 20°$ and $0° - 90°$ to determine their cyclic stability.

3. RESULTS AND DISCUSSION

3.1 *Simulation Result*

The simulation results of the bending-resistance characteristics of the functional layer of the 1# sensor sample are shown in Figure 3. The degree of resistance change varies with different bending angles, and the resistance change is greater when the bending angle is larger. As shown in Fig. 3(a), when bending at 30°, the stress is mainly distributed at the bending site and the stress on the bending surface can be neglected, resulting in a relatively large resistance change there. During the bending process at 60°, the force is unevenly distributed with the force being concentrated on one side of the bending surface as shown in Fig. 3(b); the parts with larger resistance changes are also concentrated in areas with greater stress. When bending at 90°, the force on the entire bending surface is more balanced as shown in Fig. 3(f); the resistance change averages around 0.5×10^5 Ω. When bending at 60° and 90°, as shown in Fig. 3(b), the stress cloud diagram exhibits an uneven phenomenon, which may be due to the material's properties being spatially nonuniform or the occurrence of nonuniform deformation during the deformation process.

The simulation results of the bending-resistance characteristics of the functional layer of the 2# sensor sample are shown in Figure 4. As depicted in Fig. 4(a), when bending at 30°, the force on the bending surface is uneven with the main force concentrated at the bending site, where the stress is approximately 1 N/m^2 on average. The resistance change on the bending surface is also uneven with the resistance change being maintained around 1.2×10^5 Ω. When bending at 60°, as shown in Fig. 4(b), the force on the entire bending surface is more balanced, and the resistance change is maintained within a certain range. At 90° of bending, as shown in Fig. 4(c), the stress on the bending surface is greater, and the resistance change is also the largest, with an average resistance change of about 1.3×10^5 Ω. At different bending angles, the location where the maximum stress is generated is at the bending site, and the corresponding resistance change is also the greatest. Compared with the 1# sensor sample, the functional layer prepared with this ratio exhibits a more uniform stress cloud diagram when bending at 30°, 60°, and 90°, as shown in Fig. 4(d)–(f), with greater stress on the bending surface and a larger resistance change.

Figure 5 shows the simulation results of the bending-resistance characteristics of the functional layer of the 3# sensor sample. It can be observed from Fig. 5 that during the process of bending at 30°, 60°, and 90°, as shown in Fig. 5(a)–(c), the areas with the greatest stress are mainly concentrated at the bending site, and the positions with the greatest resistance change are also at the bending site. The stress cloud diagram across the entire bending surface is relatively flat, indicating that the force on the entire bending surface is quite balanced, and the resistance change is maintained within a certain range. As seen in Fig. 5(d)–(f),

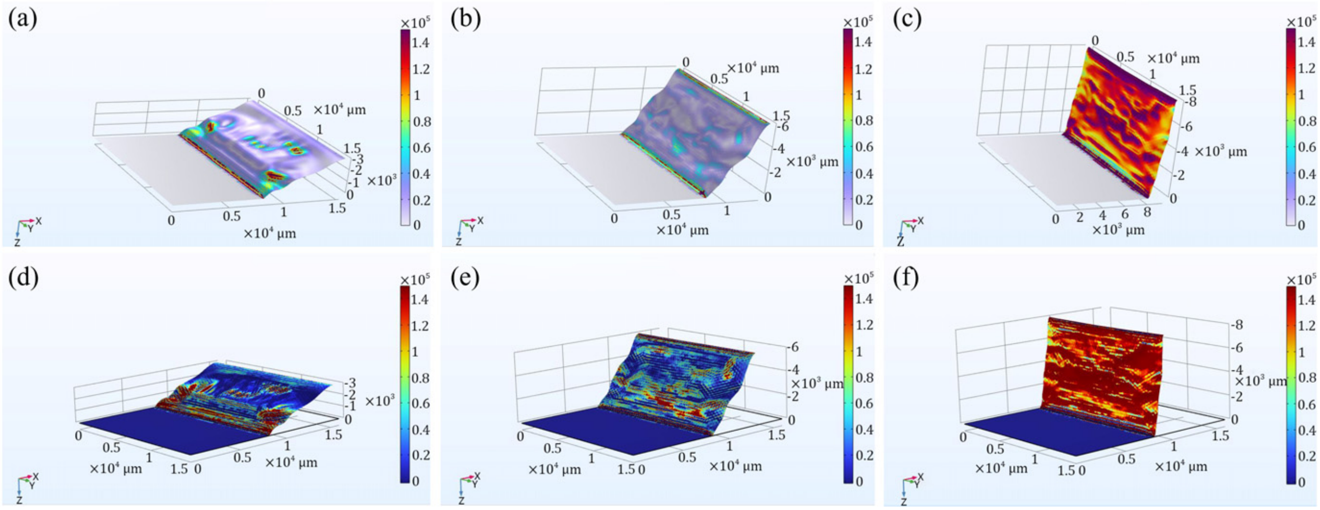

Figure 4. Simulation results of the bending-resistance characteristics of 2# sensor sample: (a) 30° bending stress diagram, (b) 60° bending stress diagram, (c) 90° bending stress diagram, (d) 30° bending-resistance change diagram, (e) 60° bending-resistance change diagram, and (f) 90° bending-resistance change diagram.

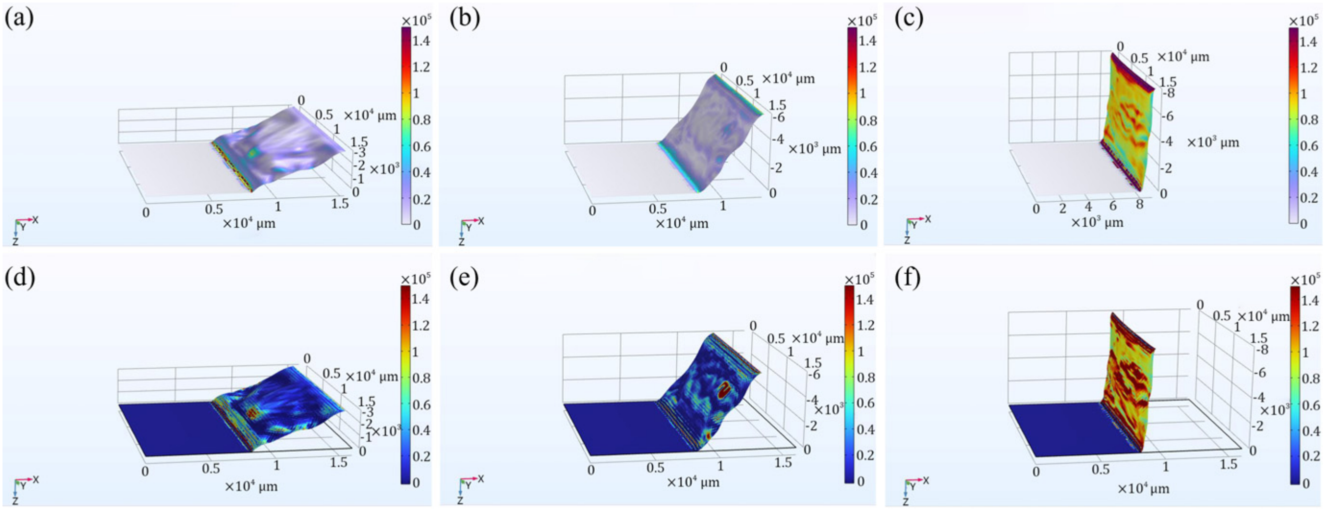

Figure 5. Simulation results of the bending-resistance characteristics of 3# sensor sample: (a) 30° bending stress diagram, (b) 60° bending stress diagram, (c) 90° bending stress diagram, (d) 30° bending-resistance change diagram, (e) 60° bending-resistance change diagram, and (f) 90° bending-resistance change diagram.

compared to bending at 30° and 60°, the stress on the bending surface is greater when bending at 90° with the stress magnitude being around 0.9×10^5 N/m^2, and the resistance change maintained around 1×10^3 Ω is also greater under this bending condition.

Figure 6 illustrates the simulation outcomes for the bending-resistance characteristics of the functional layer of 3# sensor samples. In Fig. 6(a), when bending at 30°, the stress distribution appears more uneven, indicating a more pronounced uneven force distribution. The resistance change on the bending surface is also uneven, which might be attributed to the inaccurate simulation of loading conditions, failing to account for potential nonlinear effects, leading to an uneven stress distribution. In Fig. 6(b), (c), during the bending process at 60° and 90°, the force on the entire bending surface is more evenly distributed, with higher forces at the bending site and the top of the bending surface. Overall, the resistance change is kept within a certain range.

Figure 7 displays the simulation outcomes for the bending-resistance characteristics of the functional layer of the 5# sensor. From the figure, it is evident that throughout the bending process at angles of 30°, 60°, and 90°, the force distribution across the entire bending surface is relatively even, and the resistance variation is kept within a specific range. The regions experiencing the highest stress are predominantly located at the bend, where the resistance variation is also comparatively greater.

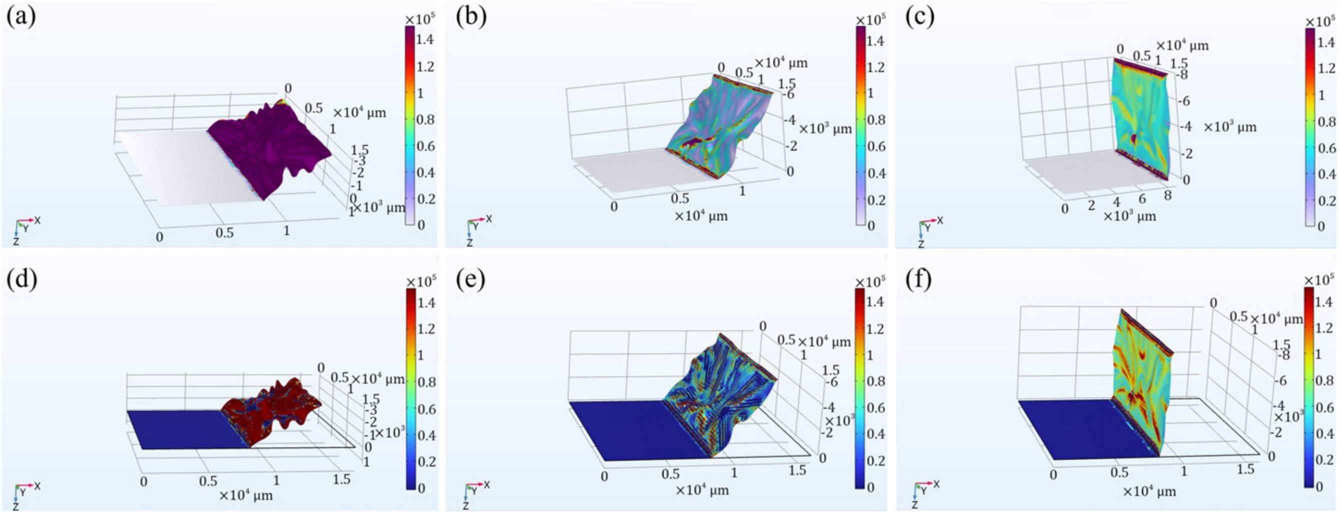

Figure 6. Simulation results of the bending-resistance characteristics of 4# sensor sample: (a) 30° bending stress diagram, (b) 60° bending stress diagram, (c) 90° bending stress diagram, (d) 30° bending-resistance change diagram, (e) 60° bending-resistance change diagram, and (f) 90° bending-resistance change diagram.

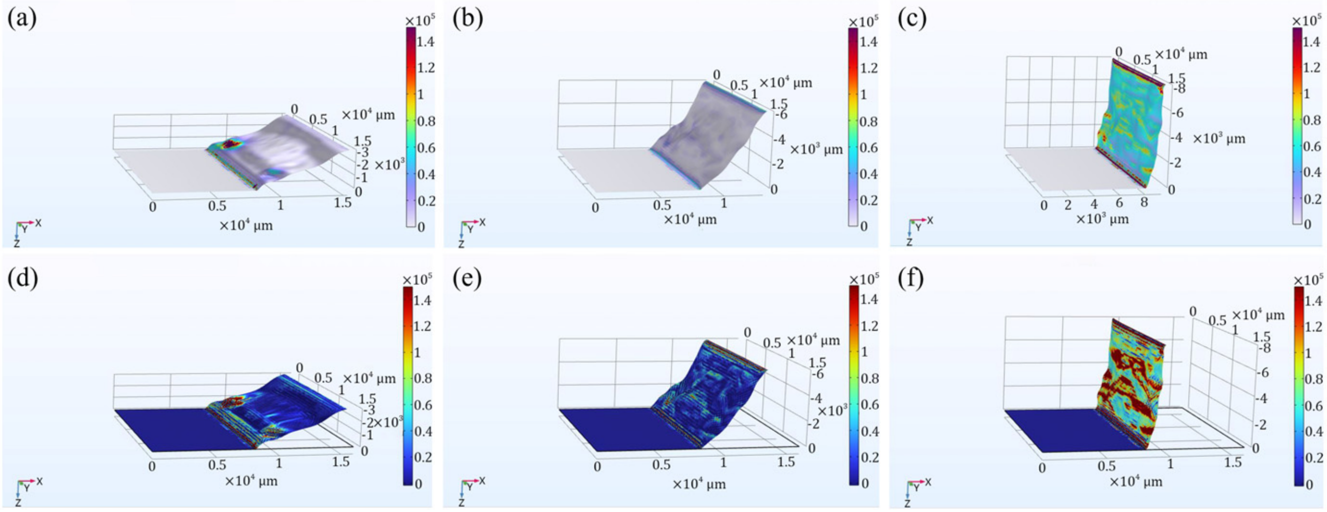

Figure 7. Simulation results of the bending-resistance characteristics of 5# sensor sample: (a) 30° bending stress diagram, (b) 60° bending stress diagram, (c) 90° bending stress diagram, (d) 30° bending-resistance change diagram, (e) 60° bending-resistance change diagram, and (f) 90° bending-resistance change diagram.

Based on the aforementioned simulation results, it can be known that bending strain of the functional layer will cause changes in resistance, and the resistance increases with increase in bending angle during the bending process. Among these five groups with different mass ratios of carbon black to graphene, when the mass ratio of carbon black to graphene is 2:1, the stress distribution is flat. In addition, the resistance changes significantly as the bending angle increases during the bending process, indicating that the functional layer prepared with a carbon black to graphene mass ratio of 2:1 has the best bending-resistance characteristics.

3.2 *Properties of Flexible Sensors*

From the simulation results, it can be seen that when the mass ratio of carbon black to graphene is 2:1, the resistance value of the functional layer changes more with the variation in bending angle, indicating that the functional layer prepared at this mass ratio has a good bending-resistance characteristic. To verify the accuracy of the simulation results, sensors with five different functional layer ratios were connected to a digital multimeter to test their resistance change rate at different bending angles to assess their sensitivity. The experimental results, as shown in Figure 8(a), indicate that when the mass ratio of carbon black to graphene in the functional layer is 2:1, the sensor has

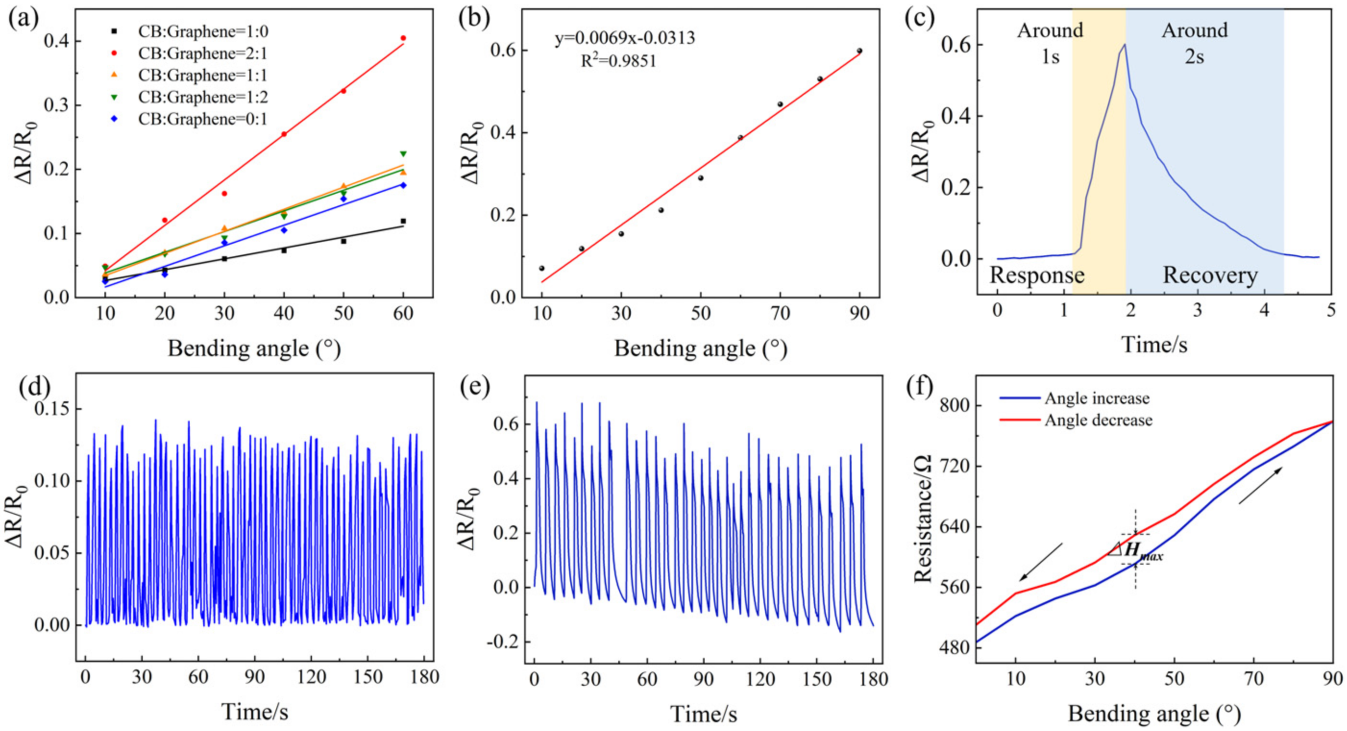

Figure 8. Performance testing of flexible sensors: (a) resistance change rate, (b) linearity, (c) response characteristics, (d) 20° bending cycle stability, (e) 90° bending cycle stability, and (f) hysteresis test. CB stands for carbon black.

the highest resistance change rate, which means the highest sensitivity. The experimental results are consistent with the simulation results.

Therefore, the bending-resistance characteristics of the flexible sensor prepared when the mass ratio of carbon black to graphene is 2:1 were further explored. It can be found from Fig. 8(b) that the resistance value of the flexible sensor increases with increase in bending angle, and the fitting curve equation of bending is $y = 0.0069x - 0.0313$ with a linear correlation coefficient of 0.9851, indicating that this flexible bending sensor has good linearity. The response characteristics of the flexible sensor from 0° to 90° are shown in Fig. 8(c). When the sensor is bent from a horizontal state to 90°, it tends to stabilize after about 1 s. When the bent sensor is restored from 90° to the original state, it takes about 2 s for the resistance change rate to return to the initial value. Therefore, the response time and recovery time of the flexible sensor when bending are approximately 1 and 2 s, respectively, indicating that this bending sensor has good response and recovery times.

Additionally, the cyclic stability of the flexible sensor was studied. The functional layer of the flexible sensor was bent to a certain angle and then restored to the initial horizontal state. It was then bent again and restored to the horizontal state, and this bending and restoring process was repeated for 180 s to test the flexible sensor through cyclic bending from 0° to 20° and from 0° to 90°. The test results are shown in Fig. 8(d) and (e), respectively. During the cyclic bending tests at angles of $0°-20°$ and $0°-90°$, the sensor was able to complete multiple bending repetitions within 180 s, and the bending performance of the sensor maintained good stability. The resistance change rate of the sensor before and after cycling showed a high degree of repeatability, and it can be seen from the figures that as the number of bending cycles increased, the resistance change rate of the flexible bending sensor fluctuated around a certain value and overall tended to be stable. However, compared to the repeated bending at $0°-20°$, the number of cycles at $0°-90°$ repeated bending decreased. Finally, the hysteresis characteristics of the flexible sensor were studied, and it can be observed from Fig. 8(f) that during the process of the sensor being gradually bent and the process of bending release, the resistance change of the sensor at the corresponding angles was not significantly different, with the maximum hysteresis of about 4.88% at 40°, indicating good hysteresis characteristics.

4. CONCLUSIONS

In this study, COMSOL Multiphysics 6.0 software was used to simulate and analyze the resistance change of the carbon black/graphene/PDMS functional layer. It was found that when the mass ratio of carbon black to graphene is 2:1, the sensor exhibits the best bending-resistance characteristics. Based on this optimized ratio, a flexible sensor was successfully fabricated using screen-printing technology, and its performance was tested. The test results show that the prepared sensor has high linearity ($R^2 = 0.9851$), fast response and recovery time (approximately 1 and 2 s, respectively), low hysteresis (4.88%), and good cyclic stability under repeated bending at small angles. These experimental results are basically consistent with the simulation results, confirming the excellent performance of the prepared sensor in detecting bending changes. In summary, the simulation analysis method proposed is applicable to the performance prediction and analysis of bending-resistance-type flexible sensors, providing guidance for the future design and application of flexible sensors.

ACKNOWLEDGMENT

This work was supported by the National Natural Science Foundation of China (No. 51902294); China Postdoctoral Science Foundation (No. 2020M670699); Shanxi Provincial Patent Transformation Special Plan Project (No. 20240012); Opening Foundation of Key Laboratory of Safety and Risk Management on Transport Infrastructures for Ministry of Transport (No. 2023KFKT016); Opening Foundation of Shanxi Provincial Key Laboratory for Advanced Manufacturing Technology (No. XJZZ202201).

REFERENCES

[1] G. Liu, Z. Zhang, Z. Li, L. Guo, and L. Ning, "0D–2D carbon-based materials in flexible strain sensors: recent advances and perspectives," 2D Mater. **10**, 22002 (2023).

[2] X. Chen, F. Wang, L. Shu, X. Tao, L. Wei, X. Xu, Q. Zeng, and G. Huang, "A single-material-printed, low-cost design for a carbon-based fabric strain sensor," Mater. Design **221**, 110926 (2022).

[3] W. Heng, G. Yang, W. S. Kim, and K. Xu, "Emerging wearable flexible sensors for sweat analysis," Bio-Des. Manuf. **5**, 64–84 (2022).

[4] R. Thankappan, K. G. Vasanthakumari, and U. M. Uzma Sulthana, "MXene-coated flexible PVDF membrane as wearable strain sensor," J. Mater. Sci.: Mater. Electron. **33**, 24542–24549 (2022).

[5] J.-K. Song, D. Son, J. Kim, Y.-J. Yoo, G.-J. Lee, L. Wang, M.-K. Choi, J. Yang, M. Lee, K. Do, J.-H. Koo, N. Lu, J.-H. Kim, T. Hyeon, Y.-M. Song, and D.-H. Kim, "Wearable force touch sensor array using a flexible and transparent electrode," Adv. Funct. Mater. **27**, 1605286 (2017).

[6] J. Ji, C. Zhang, S. Yang, Y. Liu, J. Wang, and Z. Shi, "High sensitivity and a wide sensing range flexible strain sensor based on the V-groove/wrinkles hierarchical array," ACS Appl. Mater. Interfaces **14**, 24059–24066 (2022).

[7] S.-D. Wu, S.-H. Hsu, B. Ketelsen, S. C. Bittinger, H. Schlicke, H. Weller, and T. Vossmeyer, "Fabrication of eco-friendly wearable strain sensor arrays via facile contact printing for healthcare applications," Small Methods **7**, 2300170 (2023).

[8] H. Dong, J. Sun, X. Liu, X. Jiang, and S. Lu, "Highly sensitive and stretchable MXene/CNTs/TPU composite strain sensor with Bilayer conductive structure for human motion detection," ACS Appl. Mater. Interfaces **14**, 15504–15516 (2022).

[9] L. Zhang, H. Li, X. Lai, T. Gao, and X. Zeng, "Three-dimensional binary-conductive-network silver nanowires@thiolated graphene foam-based room-temperature self-healable strain sensor for human motion detection," ACS Appl. Mater. Interfaces **12**, 44360–44370 (2020).

[10] X. Zhang, D. Xiang, Y. Wu, E. Harkin-Jones, J. Shen, Y. Ye, W. Tan, J. Wang, P. Wang, C. Zhao, and Y. Li, "High-performance flexible strain sensors based on biaxially stretched conductive polymer composites with carbon nanotubes immobilized on reduced graphene oxide," Compos. Part A: Appl. Sci. Manuf. **151**, 106665 (2021).

[11] D. Chen, Y. Cai, L. Cheng, S. Guo, T. Liu, S. Huang, H. Yu, Y. Wang, Z. Hu, and D. Gui, "Structure and function design of carbon nanotube-based flexible strain sensors and their application," Measurement **225**, 113992 (2024).

[12] P. Li, Z. Li, H. Chen, Y. Zhu, D. Yang, and Y. Hou, "Graphene-based flexible strain sensor based on PDMS for strain detection of steel wire core conveyor belt joints," Sensors **23**, 7473 (2023).

[13] N. Xu, Z. Tang, Y.-P. Jiang, J. Fang, L. Zhang, X. Lai, Q.-J. Sun, J.-M. Fan, X.-G. Tang, Q.-X. Liu, and J.-K. Jian, "Highly sensitive ratiometric fluorescent flexible sensor based on the RhB@ZIF-8@PVDF mixed-matrix membrane for broad-spectrum antibiotic detection," ACS Appl. Mater. Interfaces **15**, 52993–53002 (2023).

[14] W. Qin, J. Geng, C. Lin, G. Li, H. Peng, Y. Xue, B. Zhou, and G. Liu, "Flexible multifunctional TPU strain sensors with improved sensitivity and wide sensing range based on MXene/AgNWs," J. Mater. Sci.: Mater. Electron. **34**, 564 (2023).

[15] L. Duan, D. R. D'Hooge, and L. Cardon, "Recent progress on flexible and stretchable piezoresistive strain sensors: from design to application," Prog. Mater. Sci. **114**, 100617 (2020).

[16] Y. Yi, A. Samara, and B. Wang, "A new approach for an ultra-thin piezoresistive sensor based on solidified carbon ink film," J. Mater. Sci. **56**, 607–614 (2021).

[17] F. Zhang, S. Wu, S. Peng, Z. Sha, and C. Wang, "Synergism of binary carbon nanofibres and graphene nanoplates in improving sensitivity and stability of stretchable strain sensors," Compos. Sci. Technol. **172**, 7–16 (2019).

[18] Y. Xiao, S. Jiang, Y. Li, and W. Zhang, "Highly sensitive printed crack-enhanced strain sensor as dual-directional bending detector," Smart Mater. Struct. **29**, 45023 (2020).

[19] Y. Long, P. He, R. Xu, T. Hayasaka, Z. Shao, J. Zhong, and L. Lin, "Molybdenum-carbide-graphene composites for paper-based strain and acoustic pressure sensors," Carbon **157**, 594–601 (2020).

[20] J. Liu, F. Zhao, Q. Tao, J. Cao, Y. Yu, and X. Zhang, "Visualized simulation for the nanostructure design of flexible strain sensors: from a numerical model to experimental verification," Mater. Horiz. **6**, 1892–1898 (2019).

[21] X. Xia, Z. Xiang, Z. Gao, S. Hu, W. Zhang, R. Long, Y. Du, Y. Liu, Y. Wu, W. Li, J. Shang, and R.-W. Li, "Structural design and DLP 3D printing preparation of high strain stable flexible pressure sensors," Adv. Sci. 2304409 (2023).

[22] S. Kouchakzadeh and K. Narooei, "Simulation of piezoresistance and deformation behavior of a flexible 3D printed sensor considering the nonlinear mechanical behavior of materials," Sensors Actuators A **332**, 113214 (2021).